

The Impact of Tissue Morphology, Cross-Section and Turgor Pressure on the Mechanical Properties of the Leaf Petiole in Plants

Tanvir Rahman Faisal¹, Ehsan M. Khalil Abad¹, Nicolay Hristozov², Damiano Pasini¹

1. Department of Mechanical Engineering, McGill University, 817 Sherbrooke Street West, Montreal, Quebec H3A 2K6, Canada

2. Department of Biology, McGill University, 1205 Docteur Penfield, Montreal, Quebec H3A 1B1, Canada

Abstract

This paper describes a study of petiole structural morphology in which tissue materials, cross-sectional geometry, layer-architecture and hydrostatic condition are variables that affect the overall structural properties of the organ. *Philodendron melinonii* is selected as a model species for characterizing the mechanical properties of the petiole. The shape of the petiole is modeled through the polar parameterization of the Lamé's curves, i.e. Giell's formulation. A multiscale model of bending stiffness is proposed to capture the impact of changing the constituent tissues and the cross-sectional geometry. Stiffness and density of different tissues are used to plot the domain bounded by the limiting curve of the respective tissue material. Shape parameters and the respective tissue properties are used to generate structural efficiency maps displaying property domains within which fall all possible combinations of tissues that are shaped into a certain geometry during growth. The turgor pressure is also taken into account to show how the domain of the effective material properties changes with water content. Finite element analysis besides experimental data is used to validate the theoretical results. The maps may offer a source of inspiration for biomimetic design, as they help to gain insight into the efficiency of biological beams described by different tissues properties, geometry and turgidity.

Keywords: leaf petiole, structural hierarchy, turgor pressure, shape transformer

Copyright © 2010, Jilin University. Published by Elsevier Limited and Science Press. All rights reserved.

doi: 10.1016/S1672-6529(09)60212-2

1 Introduction

Nature exhibits many excellent examples of load bearing structures. The petiole in plants is one of the most efficient structures abundantly available in nature. Over the course of its life cycle, a plant may develop roots, stems, branches, leaves and eventually flowers and fruits. These biological organs work in synergy to ensure the survival and reproduction of the organism. The primary function of the leaf is to harvest light needed to drive the photosynthetic process, essential for the synthesis of organic compounds^[1]. The petiole is an organ that serves to attach the leaf to the stem. The word “petiole” comes from the Latin word “*petiolus*”, which literally translates into “little foot”. The petiole allows the leaf to extend outward from the plant, which can improve its ability to harvest light. In addition, the vascular tissues running through this organ allow it to conduct water and nutrients to and from the leaf.

Evolutionary processes shape the morphology of all plant organs. Over generations, natural selection has driven the evolution of efficient and structurally sound petioles. The petiole resembles a cantilever beam that supports the leaf against gravity, exposing it to the sun (Fig. 1). Under the action of wind, a petiole acts as a beam that resists the drag acting on the frontal area of the leaf exposed to wind. The petiole thus provides mechanical support against the weight of the leaf and against environmental factors such as rain and wind, resisting both bending and twisting load^[2].

The petiole can be considered as a hierarchical structure, having structural features defined at multiple length scales. At each level of the hierarchy, the elements repeat themselves to form ordered patterns. The architecture of the ordered patterns, as well as the nesting of the patterns into each other, makes a crucial contribution to the overall mechanical properties of the organ. The cross-section of the petiole (Fig. 2 shows the

Corresponding author: Damiano Pasini

E-mail: damiano.pasini@mcgill.ca

“C” shaped *Philodendron melinonii* petiole) can vary considerably between species, possessing for example a terete (tapered cylindrical), “U”, “C” or “D” shape. The “U” and “C” cross-sections are also called *sulcate* or *canaliculated*, as a groove or a “canal” appears to run longitudinally along the organ. A petiole may also have a quadrangular or hexagonal cross-section, and may possess striations^[3].

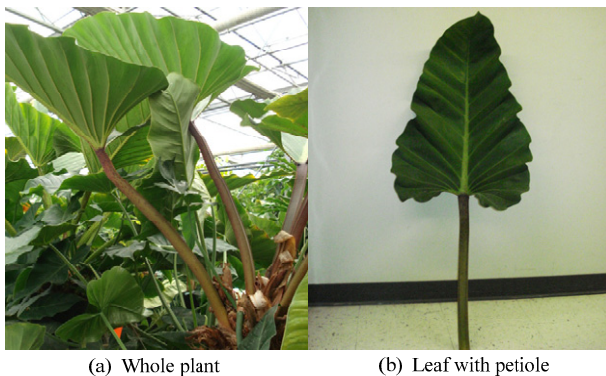


Fig. 1 *Philodendron melinonii*: whole plant and leaf with petiole.

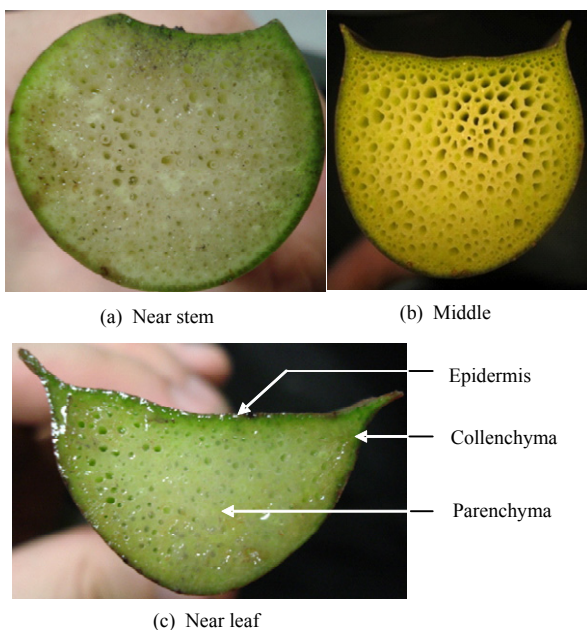


Fig. 2 *P. Melinonii* petiole cross sections at different locations along the length.

The biomechanical properties of the petiole govern its ability to support the leaf against gravity and wind^[4-8]. Broadly speaking, this organ is composed of fibrous composite biomaterials consisting of three integrated tissues: epidermis, collenchyma and parenchyma. Each of these is distinguishable in terms of its function and its material properties. The material and the geometric

properties of each tissue may play a role in governing the flexural stiffness and torsional rigidity of the whole organ. The ability of an organism to resist deformation by an imposed load depends on both the shape of its body and the mechanical properties of its tissues^[9]. The effect of cross-sectional geometry on the mechanical properties of structures has been widely studied^[10-11]. Shape transformers^[10] and shape factors^[11] are two main criteria used to study this relationship. Using shape factors, the geometry of a cross section is compared with a square of the same area. Using shape transformers, the cross-sectional geometry is compared with a rectangle that envelops a given cross section. While shape factor depend on both size and shape of a cross section, shape and size are decoupled when using shape transformers. Shape transformers thus provide a better approach for investigating the geometric effect of cross-sectional shape on the mechanical properties of a structure.

Multiscale modeling based on continuum mechanics can be used to capture the influence of cross-sectional geometry. The compliant properties of natural shapes are plotted on maps for comparison with several petiole specimens^[12]. Multilayered structures can display superior mechanical performance over monolithic materials. Bi-material sandwich beams are frequently used in different micro systems. A flexural stiffness domain for a tri-material laminate system has been proposed for different layered architectures^[13]. This efficiency map provides the boundary domain for all possible material combinations and an effective approximation for the conceptual design stage. Using this technique, it is possible to draw an efficiency map of the flexural stiffness in the petiole.

As a living organ, the petiole of any plant consists largely of water, with turgor pressure influencing the overall effective modulus. Increased turgor pressure can result in increased tissue stiffness^[14-15]. Pitt *et al.* modeled plant tissues as fluid filled cellular structures and established a relationship between stiffness and turgor pressure^[16]. More recently, carrot tissue was modeled as a closed-cell liquid-filled foam, displaying a linear relationship between turgor pressure and stiffness^[17].

In this study, shape transformers are employed to study the influence of cross-sectional geometry at different levels of the structural hierarchy of the petiole. This method is also used for cellular structures, the macro-scale properties of which are highly dependent on

their microstructure. A finite element model is developed to elucidate the relationship between bending stiffness and the cell radius to cell thickness ratio of the petiole microstructure. The mathematical model is compared with experimental results and is used to develop structural efficiency maps that capture the effect of turgor pressure in parenchyma tissue on the effective flexural stiffness and torsional rigidity of the whole petiole.

2 Materials and methods

2.1 Morphology of *Philodendron melinonii*

Philodendron melinonii was first found in the rain forests of French Guiana, Suriname, Venezuela, and Northern Brazil. *Philodendron melinonii* is both terrestrial and epiphytic. An epiphytic species is one capable of growing on the branch of a tree or climbing a tree to better collect sunlight. Epiphytic individuals of this species grow on trees just under the canopy where they may be subjected to significant wind load. The leaves and petioles of *Philodendron melinonii* can grow quite large. The petiole and leaf are nearly equal in length, each growing to approximately 28 inches (70 cm). A fully grown individual can reach approximately eight feet in diameter (2.5 m). Fig. 1 shows typical *P. melinonii* leaf and petiole. The petiole is somewhat spongy to the touch. In cross section, it is shaped like a rotated capital letter “D” or sunken on the upper surface to resemble the capital letter “C”.

2.2 Constituent tissues in petiole

2.2.1 Epidermis

The epidermis is the dermal tissue system of leaves, petioles, stems, roots and others. It is the outermost cell layer of the primary plant body. The cells of the epidermis are structurally and functionally variable. Most plants have an epidermis that is single cell layer thick. Epidermal cells are tightly linked to each other and provide mechanical strength and protection to the plant^[18].

2.2.2 Collenchyma

The collenchyma is the ground tissue that is strong in tension, composed of elongated cells with unevenly thickened walls. It provides structural support, particularly in growing roots and leaves. The location and type of collenchyma cells vary across species^[19].

2.2.3 Parenchyma

Parenchyma is among the most common ground tissues and parenchyma cells are the most primitive type in plants. They usually lack secondary cell walls, possessing only thin primary cell walls. These cells vary considerably in morphology^[20].

2.3 Hierarchies in petiole structure

The structure of the petiole is adapted to meet multiple evolving requirements. Besides sustaining metabolic functions, it provides structural support. The internal structure of certain organs exhibits complex but repeated ordered organization at each length scale. These hierarchical levels are nested in one another, as observed in trabecular bones, wood and tendon. For example, in the *Euplectella aspergillum*, a deepwater sponge, six hierarchical levels have been identified^[21]. These levels range from nanoscale to macroscopic scale. Each level possesses a structural design of a particular order that forms at different growth phases. In this case, the assembly consists of a three-dimensional cylindrical lattice structure, where the interaction of the structural motifs at each order plays a crucial role. Material structuring confers remarkable physical properties, such as strength, toughness and resilience, with minimum material use. Fig. 2 shows the *P. melinonii* petiole cross sections at different locations along the petiole length. The cross sections show the visible cellular structure which varies in density along the length of the petiole.

Although the petiole can consist of a variety of tissues, including sclerenchyma, phloem and xylem, for the purposes of this paper, we simplify it into a three-tissue system. These three tissues, that is parenchyma, collenchyma and epidermis, contribute most to the total mass of the organ. Each tissue has distinct characteristics, with patterns that vary among species. Although the largest size structure of the hierarchy often plays the most relevant role, each hierarchy contributes to the overall mechanical performance. The next section proposes a scheme to characterize the effect of such material hierarchies, as shown in Fig. 3. From the figure it can be observed that the microstructure of the petiole exhibits neither perfect circular nor hexagonal shape. The innermost hierarchical level, shown in Fig. 3a, exhibits a more hexagonal microstructure while others show circular or combination of both.

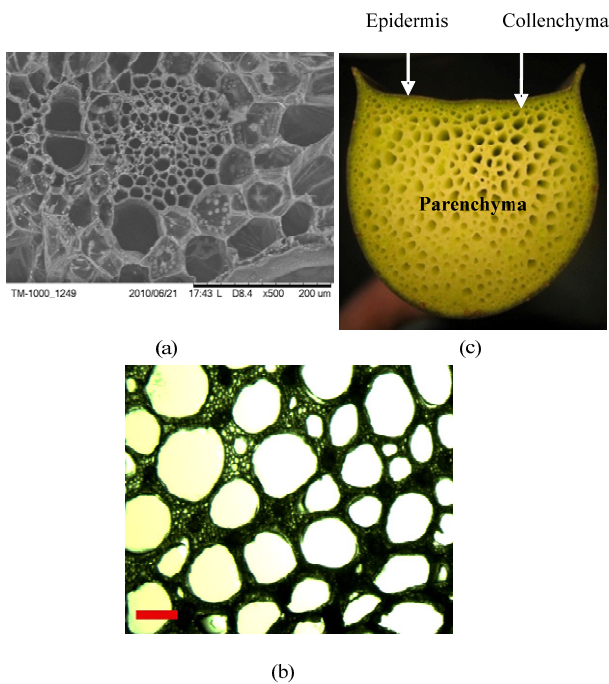


Fig. 3 Images of petiole hierarchy at different length scales; (a) scanning electron micrograph of parenchyma tissue, (b) light micrograph of parenchyma tissue and (c) photograph of whole petiole cross section.

2.4 Modeling hierarchical structure with shape transformers

Provided the appropriate assumptions, the theory of elasticity can be applied to any length scale in a hierarchical structure. Classical mechanics is able to predict the deformation of a structural configuration at any length scale. For a multi-scale structure like the petiole, the theory can yield accurate results as long as each length scale is significantly different (at least differ by the order of 10) from those above or below it in the hierarchy.

Cross-sectional effects can be captured by using the method of shape transformers. With this method, a geometrical quantity of a cross section is normalized by the same geometrical quantity of the surrounding envelope, which is the rectangle defined by the main cross section size. The shape transformer of a geometric quantity, g , is defined by:

$$\psi_g = \frac{g}{g_D}, \tag{1}$$

where g_D is the geometric quantity of the envelope. For example, shape transformers for area, second moment of area about x -axis and torsional constant can be defined as:

$$\begin{cases} \psi_A = \frac{A}{A_D} \\ \psi_{I_{xx}} = \frac{I_{xx}}{I_{xxD}} \\ \psi_{J_T} = \frac{J_T}{J_{TD}} \end{cases} \tag{2}$$

To describe the structuring effect of a material, we can examine the idealized example shown in Fig. 4b. This figure shows four hierarchical levels of a cross section where the elements are assumed to be continuous at each level of the hierarchy. At level 0, the material M_0 is uniform and shapeless. When shaped, M_0 becomes a solid circular two-dimensional structure. During this process, M_0 is conferred with geometrical properties G_1 and M_1 , i.e. the shaped material at level $n = 1$, inherit properties M_0G_1 . As an example, we apply the scheme of shape transformers, ψ_G , to the bending stiffness^[12,22-23]. The effective flexural properties E_1 at the first hierarchical order are obtained by normalizing E_0I_1 with the envelope property I_{D1} :

$$E_1 = E_0 \frac{I_1}{I_{D1}} = E_0 \psi_I^1. \tag{3}$$

At the following level, the circular elements of the first level are clustered together to form a hollow rectangular cross section. Assuming that the circular elements of the first level show isotropic and uniform material properties, similar to the first level, at the second level ($n = 2$) it can be expressed as:

$$\psi_I^2 = E_0 \psi_I^1 \psi_I^2. \tag{4}$$

Hence the structure of two hierarchical levels is factored in by the shape properties. This can lead to the determination of the effective material properties. Further structuring of the cells in the previous level results

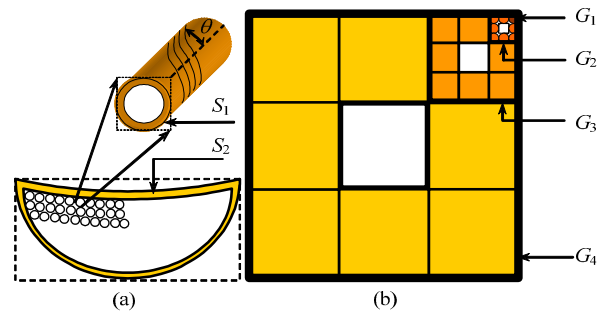


Fig. 4 (a) Structural hierarchies of a petiole; (b) an ideal cross-section structure^[12].

in an effective Young's modulus at level 3 that is expressed as:

$$E_3 = E_2 \psi_1^3 = E_0 \psi_1^1 \psi_1^2 \psi_1^3. \quad (5)$$

If the process repeats at higher levels, the effective Young's modulus at the n th level can be expressed as:

$$\frac{E_n}{E_0} = \prod_{j=1}^n \psi_1^j. \quad (6)$$

The above relationship is a ratio of effective material properties and is valid for a single-layered material. However the petiole of *P. melinonii* is a multilayer structure where each layer has different mechanical properties.

2.5 Multi-scale model for a layered micro-structured petiole

In Fig. 3, different layers can be identified in the petiole cross section, each with its own material properties. The inner layer is a structured material of uniformly distributed hollow tubular cells. The outer is the dermal tissue, which consists of peripheral bands of lignified material. The properties of the former are described by Eq. (6). The contribution of the latter depends on the thickness of the outer coat, which is often species-specific. The material properties resulting from layering a system with k materials can be expressed in terms of shape transformers^[22]. In this case, the effective flexural modulus of a multilayered cross section can be written as:

$$E_T = \sum_{i=1}^k E_i \psi_{li}. \quad (7)$$

Replacing E_i in Eq. (7) by E_n in Eq. (6) yields:

$$E_T = \sum_{i=1}^k (E_0 \prod_{j=1}^n \psi_1^j) \psi_{li}. \quad (8)$$

Similarly we can obtain the equation for torsional stiffness,

$$J_T = \sum_{i=1}^k (J_0 \prod_{j=1}^n \psi_j^j) \psi_{ji}. \quad (9)$$

The relationship between G and E is,

$$G = \frac{E}{2(1+\nu)}, \quad (10)$$

where G is the shear modulus, J_T is the torsional constant

and ν is Poisson's ratio, which is approximately 0.3 for cellulose in plants.

Shape transformers and envelope multipliers allow for the reformulation of the equations of mechanics in terms of the factors F , M , ψ_g , g_D , where F describes the functional requirements, M is the material properties, ψ_g is the cross section geometry decoupled respectively in shape and size^[22,24]. Such a formulation permits the co-selection of material and shape in constrained and unconstrained design. Both cross section geometry and structured parenchyma tissue geometry are shown in Table 1. In this work, we assumed the innermost microstructure to be better replicated with the array of regular hexagons. This array is more closely packed that represents the actual hierarchy better than the circular array. Table 1 shows the formulation for the rectangular, circular and hexagonal microstructures.

The relation of E_T can be rearranged and substituted in the shape transformers expression of an equation of mechanics, $E.M.$ ^[23], which, for instance, for mass, torsional and flexural stiffness can be rewritten,

$$E.M. = F \times M_0 \times \sum_{i=1}^k (\prod_{j=1}^n S^j) S_i \times G_D. \quad (11)$$

Shape transformers in Eq. (11) were previously formulated for idealized pure geometric shapes. In this paper, the Gielis parameterization of the Lamé' curves^[25] has been introduced to redefine their formulation for biological cross-sectional shapes. This enables the accurate representation of natural forms and is used here to capture the last hierarchy of the petiole, i.e. the hollow grooved contour. In polar coordinates (r, ϕ) , the shape contour is given by:

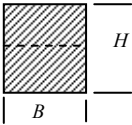
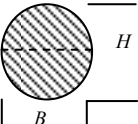
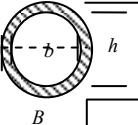
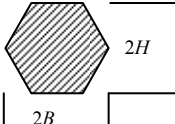
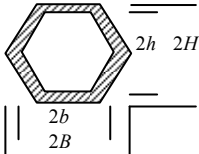
$$r = f(\phi) \frac{1}{\sqrt[n_1]{(|\frac{1}{a} \cos(\frac{4}{m} \phi)|)^{n_2} + (|\frac{1}{b} \sin(\frac{4}{m} \phi)|)^{n_3}}}. \quad (12)$$

The parameters a , b , m , n_1 , n_2 , n_3 are used to plot the shape contours of *Philodendron melinonii*, and are 0.6, 1.8, 8, 250, 115, 75, respectively.

2.6 Flexural modulus of three-tissue multilayered petiole

To characterize the flexural modulus of a three tissue system, we consider as design variables the material properties of the layers, the shape and size of the cross-section, the architecture and the number of the layers.

Table 1 Area (A), second moment of area (I), geometric transformation, ψ_I and ψ_A of section

Cross sectional shape	A	I	$\psi_A = \frac{A}{A_D}$	$\psi_I = \frac{I}{I_D}$
	BH	$\frac{BH^3}{12}$	1	1
	$\frac{\pi}{4}BH$	$\frac{\pi}{64}BH^3$	$\frac{\pi}{4}$	$\frac{3\pi}{16}$
	$\frac{\pi}{4}(BH - bh)$	$\frac{\pi}{64}(BH^3 - bh^3)$	$\frac{\pi}{4}\left(1 - \frac{bh}{BH}\right)$ $0 \leq \psi_A \leq \frac{\pi}{4}$	$\frac{3\pi}{16}\left(1 - \frac{bh^3}{BH^3}\right)$ $0 \leq \psi_I \leq \frac{3\pi}{16}$
	$3BH = \frac{3\sqrt{3}}{2}B^2$	$\frac{15}{18}BH^3 = \frac{5\sqrt{3}}{16}B^4$	$\frac{3}{4}$	$\frac{5}{8}$
	$3(BH - bh) = \frac{3\sqrt{3}}{2}(B^2 - b^2)$	$\frac{15}{18}(BH^3 - bh^3) = \frac{5\sqrt{3}}{16}(B^4 - b^4)$	$\frac{3}{4}\left(1 - \frac{bh}{BH}\right)$ $0 \leq \psi_A \leq \frac{3}{4}$	$\frac{5}{8}\left(1 - \frac{bh^3}{BH^3}\right)$ $0 \leq \psi_I \leq \frac{5}{8}$

The model presented here is based on the assumption that there is a perfect bonding between each layer. Although this hypothesis is too unrefined to describe the real interfacial bonding between cells and layers, it still fits the purpose of an approximate study of the constituent materials since it allows for finding limiting ideal bounds of the effective properties. The strain at the interface between materials is also assumed to remain unchanged. It is assumed that bending strain varies linearly along all the layers without any discontinuity. On the other hand, only the stress varies continuously within each layer but discontinuously at the layer transition since each material has its own modulus.

A petiole beam subjected to a pure bending moment M_B per unit width may consist of multiple material layers arranged with respect to the shape classes. The flexural stiffness and unit mass of the system can be simplified as follows:

$$\frac{M_B}{c_1} = \psi_I I_D E_D = I_D E_D, \tag{13}$$

$$\frac{m}{l} = \psi_A A_D \rho_D = A_D \rho_D, \tag{14}$$

where, c_1 is the curvature of the beam. $M_B / (I_D c_1) = E_D$ and $m / (A_D l) = \rho_D$ are, respectively, the effective properties, flexural modulus and density, of the beam. To express them as functions of the layer geometry, L_g , and their materials, we assign to the i th layer, where $i = 1, 2, \dots, k$, Young's Modulus E_i and density ρ_i , respectively, and second moment I_i of area and area A_i . Then, we express the geometry of the layer architecture in terms of the shape transformers of each layer, ψ_{Ai} and ψ_{Ii} , and write the effective properties of the system as:

$$E_D = \sum_{i=1}^k E_i \frac{I_i}{I_D} = \sum_{i=1}^k E_i \frac{\int_{A_i} y_i^2 dA}{I_D} = \sum_{i=1}^k E_i \psi_{Ii}, \tag{15}$$

$$\rho_D = \sum_{i=1}^k \rho_i \frac{A_i}{A_D} = \sum_{i=1}^k \rho_i \psi_{Ai}. \tag{16}$$

Having modeled the properties at the level of the layers, the focus is now on the next level of the structural

hierarchy, i.e. the cross-sectional geometry. We consider a beam of generic cross-section shape, S , which can have either a double axis or single axis symmetry. The transformed flexural modulus and density can be obtained by rearranging Eqs. (15) and (16), and by applying $\psi_A \neq 1$ and $\psi_I \neq 1$ to their respective properties of the envelope, E_D and ρ_D , as:

$$E_T = \frac{M_B}{c_1 I_D^2} = \psi_I E_D = \psi_I \sum_{i=1}^k E_i \psi_{Ii}, \quad (17)$$

$$\rho_T = \frac{m}{I A_D^2} = \psi_A \rho_D = \psi_A \sum_{i=1}^k \rho_i \psi_{Ai}. \quad (18)$$

The above effective properties can capture the multi-scale effect of changing the variables at different level of the structural hierarchy.

The final hierarchical level of the petiole resembles the actual shape of the organ and is a two dimensional irregular shape formulated by Gielis^[25] parameterization. In this work, the domain integral is transformed into line integral using Green's theorem. Then the integral is computed using quadratic elements that represent the coordinates over the boundary. The procedure produces exact and symbolic formulas for shapes enclosed by boundaries that can be represented by 1st or 2nd order polynomials. The integrals are used to compute various geometric properties e.g., area and inertial properties. Fig. 5 shows a two dimensional arbitrary domain in the x - y plane with continuous piece-wise boundary. The geometric and inertial properties of the domain can be obtained by integrating the following integrals,

$$A = \iint dx dy, \quad I_{xx} = \iint y^2 dx dy, \quad (19)$$

$$I_{yy} = \iint x^2 dx dy, \quad \bar{x} = \frac{A_y}{A}, \quad \bar{y} = \frac{A_x}{A},$$

where, A is area, I_{xx} is the moment of inertia about x -axis, I_{yy} is the moment of inertia about y -axis, \bar{x} and \bar{y} are the centroid of the given domain. Each one of the above integrals can be written in one of the following forms:

$$I_1 = \iint \frac{\partial F_1}{\partial x} dx dy, \quad I_2 = \iint \frac{\partial F_2}{\partial y} dx dy, \quad \text{or}$$

$$I_3 = \frac{1}{2} \iint \left(\frac{\partial F_1}{\partial x} + \frac{\partial F_2}{\partial y} \right) dx dy, \quad (20)$$

where F_1 is x , $x y^2$, and $x^3/3$ for A , I_{xx} and I_{yy} respectively. F_2 can be obtained in the same manner. Putting the integrals of Eq. (19) in each one of the three forms given

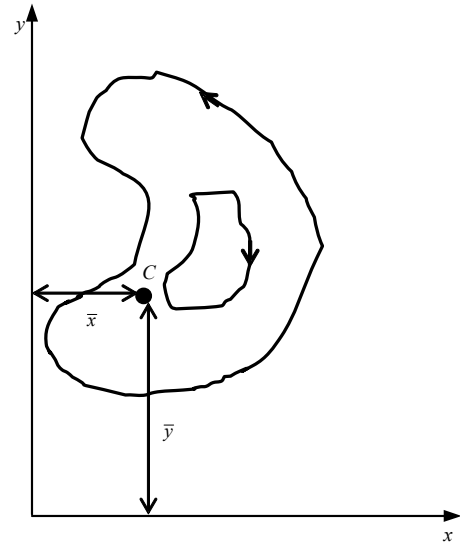


Fig. 5 2-dimensional arbitrary area with irregular boundaries.

by Eq. (20) and using the well known Green's theorem for transforming domain to boundary integrals, the following equations are obtained for each case:

$$A_1 = \oint x dy, \quad A_2 = -\oint y dx,$$

$$A_3 = \frac{1}{2} \oint (x dy - y dx), \quad (21a)$$

$$(I_{xx})_1 = \oint x y^2 dy, \quad (I_{xx})_2 = -\frac{1}{3} \oint y^3 dx,$$

$$(I_{xx})_3 = \frac{1}{2} \left(\oint x y^2 dy - \frac{1}{3} y^3 dx \right), \quad (21b)$$

$$(I_{yy})_1 = \frac{1}{3} \oint x^3 dy, \quad (I_{yy})_2 = -\oint x^2 dx,$$

$$(I_{yy})_3 = \frac{1}{2} \left(\oint \frac{1}{3} x^3 dy - x^2 y dx \right), \quad (21c)$$

where the line integration over the boundary is counter-clockwise for the exterior boundary and clockwise for the interior boundary as shown in Fig. 5. The boundary is discretized by N number of nodes and intervals. Over those intervals the integration is performed and summing up the sub-integrals yields the desired area and inertial quantities.

2.7 Modeling stiffness with turgor pressure

The parenchyma tissue contains vascular bundles which carry the nutrients, water and other fluids through the organism; thus the effect of turgidity is the highest in

parenchyma tissues. The parenchyma tissue is modeled by assuming two cell geometries for the cell: the simplest spherical cell and the regular hexagon cell (Fig. 6), surrounded by the elastic cell walls. It is observed in Fig. 3a that the fluid filled cells are nearly hexagonal in shape and very densely packed (Fig. 3). The cell walls are considered as thin elastic membranes. Each cell is filled with an incompressible fluid, which exerts a pressure P in excess of the external atmospheric pressure on the cell walls. This pressure, which corresponds to the turgor pressure in the cells of the parenchyma, is supposed to be equal in each cell of the geometric model. It is further assumed that the cell fluid cannot penetrate the walls when the parenchyma is being stretched. The cell wall material is assumed to follow Hooke's law, which describes the proportional relationship between stress and strain. Changes in turgor pressure result in cell structural changes, such that an increase in pressure gives rise to an increase in parenchyma volume. The elastic cell walls stretch in response to this pressure. In stretching a strip of material following Hooke's law from a length l to $l+\Delta l$, the potential energy stored in a volume is changed by,

$$\Delta U = \frac{1}{2} EV \left(\frac{\Delta l}{l} \right)^2, \quad (22)$$

where, E is the Young's modulus. For the cellular structure, the energy is the increased elastic energy of the cell walls due to stretching. Based on this fundamental relationship Eq. (22) Nilsson *et al.* derived an expression that relates the stiffness of parenchyma tissue to the turgor pressure^[14] as:

$$E = \left[1 + \frac{7-5\nu}{20(1+\nu)} \right] 3P + \frac{3(7-5\nu)}{10(1+\nu)} \frac{D}{r_0}, \quad (23)$$

where, D is the ratio of Young's surface modulus to $(1-\nu)$, and r_0 is the radius of cell. The above expression, further simplified, can be written for circular (spherical cell in 3D) model as:

$$E_C = 3.6P + 2.5. \quad (24)$$

The expression for the hexagonal array (tetrakaidecahedron cell in 3D) is,

$$E_H = 3.63P + 2.7, \quad (25)$$

where in both the above two expressions, P indicates the turgor pressure.

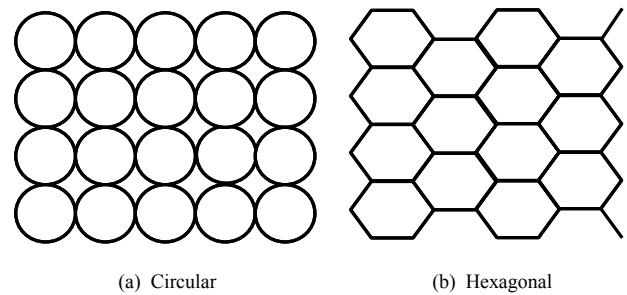


Fig. 6 Parenchyma tissue modeling based on circular and regular hexagon to evaluate turgor pressure.

2.8 Torsional and flexural testing of *P. melinonii* petioles

We collected *P. melinonii* samples from the Montreal Botanical Garden. These are grown in greenhouses at 70% humidity with a temperature varying from 22°C at night to 26°C during the day. The plants were watered with 150 ppm fertilizer, alternating between 21:5:20 and 15:0:0 N:P:K. Petioles were cut at the base and stored with the cut end in standing water to avoid dehydration. Immediately prior to testing, petioles were cut from their leaves and subsequently cut transversely into two unequal portions. The cut was consistently placed such that the proximal portion measures 35 cm in length, to ensure a reasonable length to width ratio for flexural testing. The distal portion was used for torsional testing. Before each experiment, the proximal and distal ends of the petiole were photographed in cross-section, as well as the "middle" location where the petiole was cut in two. The dimensions of these cross sections were measured using digital calipers.

An apparatus for testing the torsional and flexural stiffness of plant samples was constructed in house. Petiole portions were placed within aluminum clamps and fixed by using epoxy adhesive. During torsional testing, one of the clamps was rotated by adding weights to a pulley. During flexural testing, weights added to a second pulley would put tension on a thread attached to the middle of the sample by means of a torus-shaped steel ring. The angle of deflection caused by the addition of weight was measured using a touchless rotary sensor feeding into a digital oscilloscope. Fig. 7 shows the experimental setup.

The samples were loaded in 200 g increments up to 3 kg, although the maximum load was frequently lower in the case of more compliant samples. The mass of the

whole petioles was measured using a digital scale. The volume was estimated by measuring the displacement of water inside a graduated cylinder. These measures were used to estimate the organ density.

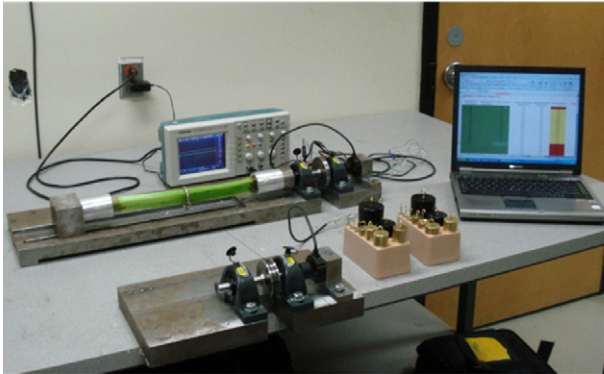


Fig. 7 Experimental setup.

3 Results and discussion

3.1 Maps describing the effective flexural modulus and density of multilayered petiole

We assumed that the petiole consists of three integrated tissues, though in reality there is no bonding between epidermis and parenchyma. In our analysis we plot the efficiency zone based on all possible combinations of these three tissue types. One aim of this paper is to create a domain within which the bending stiffness of the *P. melinonii* petiole falls. The three constituent tissues are $M_{epi}(\rho_{epi}, E_{epi})$, $M_{col}(\rho_{col}, E_{col})$, $M_{par}(\rho_{par}, E_{par})$. Fig. 8 shows five sub domains consisting of three tissues. Domain I, II, and III refer to bi-tissue systems of $M_{epi}-M_{col}$, $M_{epi}-M_{par}$, $M_{par}-M_{col}$. These actually indicate the sandwich concepts having specific property bounds. Within these, there exist all possible bi-tissue systems containing multiple layers arranged. Region IV describes properties that can be achieved by either the bi-tissue systems, $M_{epi}-M_{col}$, $M_{epi}-M_{par}$ or the tri tissue system $M_{epi}-M_{col}-M_{par}$. Domain V consequently shows the three integrated constituent tissues. The petiole flexural stiffness is expected to fall within this region as the petiole consists of the three tissues. The closed circles in the figure are experimental data from the mechanical testing of *Philodendron melinonii*. The experimental values of flexural stiffness of the petioles fall within the zone V. These values are expected to fall closer to the parenchyma tissue (zone II). However, the theoretical model does not account for all of the tissue

types normally present in a plant organ. The tissues that have been ignored, despite contributing little mass, may affect the mechanical properties in unpredicted ways. Moreover, it is assumed that there is perfect bonding between two layers which may not be realistic for the petiole morphology. The tissues of the petiole are usually considered fibrous composites, however the modelling do not take this into account.

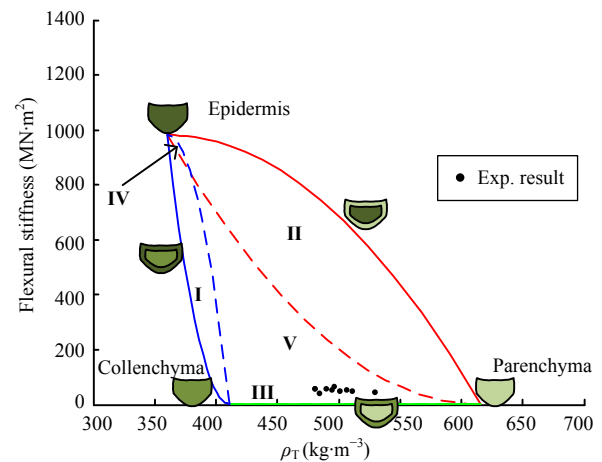


Fig. 8 Domain of flexural stiffness for epidermis-collenchyma-parenchyma tissue.

3.2 Effect of cellular microstructure in flexural stiffness

Considering a tissue as a homogeneous material can be informative, however tissues are cellular in nature and tissue density varies along the length of the petiole. The microscale cellularity of the parenchyma tissue can be observed in a cross-sectional image of the petiole (Fig. 3). Fig. 9 shows the effect of cellular structure over homogenous material properties. The solid lines depict the boundary of two-tissue (collenchyma and parenchyma) systems, considering both tissues to be homogeneous. The parenchyma tissue is cellular at two length scales, in contrast to the collenchyma tissue which is only cellular at the microscopic scale. The cellularity of parenchyma tissue will thus be a primary factor governing the mechanical properties of the whole organ. The first dashed line, closest to the solid green line, represents the stiffness of solid circular tissues that represent very densely packed parenchyma. The tissue density appears higher near the stem (base), so this line is intended to represent that part of the petiole. The line to the right of the previous one represents a structure of lower density and the outermost dotted line indicates

lower density cellular tissue, which can be considered as the middle section of petiole lengthwise. The domain is expanded for cellular microstructures compared to homogeneous tissues, and it is shifted outward with increasing r/t .

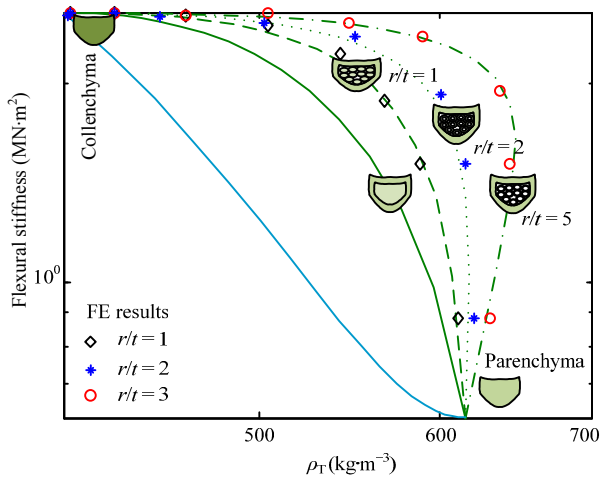


Fig. 9 Flexural stiffness of structured tissues.

FE modeling has been performed based on a two-tissue cellular system having circular microstructure. The results of the theoretical modeling are validated by finite element modeling of a micro-structured cantilever beam modeled in the finite element software ANSYS. In this model the bending stiffness of the structure, EI , is obtained by using the relationship between the tip deflection, δ , of a cantilever beam of 12 cm in length and the applied concentrated force, F . As shown in Figs. 10a and 10b, the petiole model consists of outer collenchyma layer that is tightened with connected hollow parenchyma cylinders. Here, the petiole outer layer is meshed with solid 95 element, a 3D element with 20 nodes, and the beam 4 element, a 3D beam element, is used to model the hollow parenchyma cylinders. The petiole finite element is shown in Fig. 10c. The connectivity between the parenchyma layer and the collenchyma as well as the connectivity between the collenchyma cylinders is modeled by coupling the in-plane degree of freedom of the nodes located on the inner surface of the petiole to beam nodes. All the degrees of freedom of the nodes on one of the petiole distal are taken to model the cantilever beam boundary conditions. A concentrated force of 0.2 N is applied on the petiole tip, and the corresponding beam tip deflection is obtained. The bending stiffness resulted from FE modeling is shown in Fig. 9.

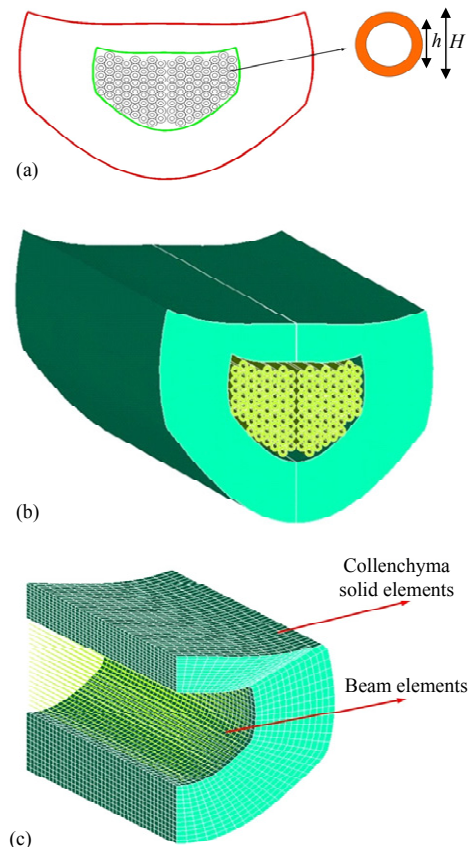


Fig. 10 FE model on ANSYS.

3.3 Effect of turgor pressure on tissue mechanical properties

The previous modeling and FE results do not include the effect of turgor pressure on the stiffness. Fig. 11 displays the effect of turgor pressure on parenchyma tissue for different types of microstructures. Effective flexural modulus appears to increase as a function of the turgor pressure, which is expected, since the stiffness of parenchyma tissue varies with the turgor pressure. Turgor pressure can have a dramatic effect on the stiffness, which can increase up to 70% compared with a baseline of no turgidity. Table 2 shows the change in flexural stiffness of parenchyma tissue with respect to turgor pressure.

Table 2 Effect of turgor pressure on stiffness of parenchyma tissue

Turgor pressure (MPa)	Increase in stiffness (%)
1	49.22
2	53.42
4	60.02
6	64.98
8	68.85
10	71.95

Fig. 11 shows also the effect of cell geometry on the flexural stiffness. Since the tetrakaidecahedron (hexagonal) cells are more closely packed than the spherical (circular) cell forms, tissues of the former structure will generally be stiffer than tissues of the latter structure. Although the model presented in section 2.7 and used here to generate this map is simplified, it is capable of capturing the effect of turgidity with a good approximation of the same order of magnitude as the approximate theoretical value^[14]. It is worth mentioning that the effect of turgor pressure does not change for both the flexural and torsional stiffness. Table 2 indicates the % gain in both torsional and flexural stiffness. In Fig. 12 the domain of flexural stiffness has been shown in log scale with the effect of turgor pressure. The turgor pressure impacts the effective flexural modulus of the parenchyma-collenchyma domain.

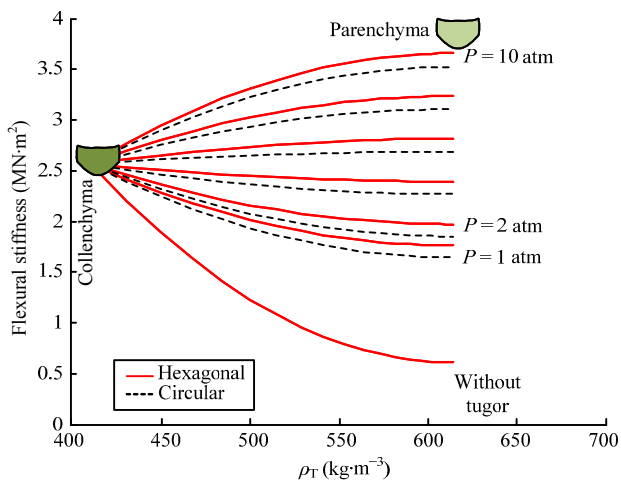


Fig. 11 Effect of turgor pressure on the flexural stiffness within parenchyma tissue.

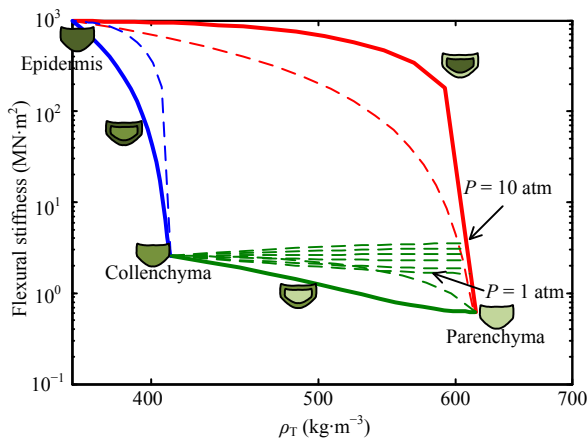


Fig. 12 Turgor pressure on the complete petiole (3 tissue) domain.

3.4 Maps describing the effective torsional modulus and density of multilayered petiole

Fig. 13 shows the domain of the torsional stiffness. Similar to the domain of flexural stiffness with a three-tissue system, this domain is more compact than the previous domain. The experimental results for torsional stiffness lie closer to the boundary of the epidermis and parenchyma domain. The collenchyma tissue is stronger in tension but not in twisting load. Hence the experimental results are closer to the region of epidermis-parenchyma. But in reality there is no bonding between epidermis-parenchyma tissues. So, it can be deduced that the torsional stiffness largely depends on the epidermis tissue, which is rigid to twisting load. The epidermis tissue is stiffer than the other two tissue types. The stiffer epidermis appears to play a key role in controlling torsional stiffness rather than flexural stiffness.

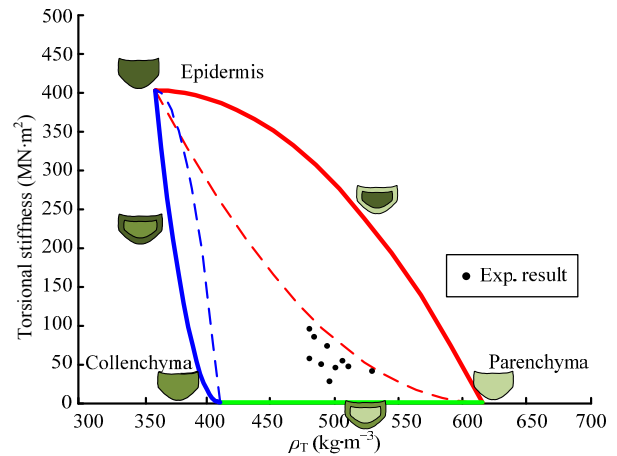


Fig. 13 Domain of torsional stiffness for epidermis-collenchyma-parenchyma tissues.

4 Conclusion

The leaf petiole, like many biological structures, is a hierarchical cellular solid. At the microscopic scale, this organ consists of fluid filled cells bounded by cell walls. The parenchyma tissue also exhibits cellularity at a higher length scale with air-filled intercellular spaces at the millimeter scale air filled pores on the order of millimeters. Here only the parenchyma tissue is considered as a cellular structure, although the other tissues are cellular at the microscopic level. This type of modeling can be extended to such microscopic cellular structures in future work. Turgor pressure has a dramatic

effect on the tissue properties as well as mechanical properties, increasing torsional and flexural stiffness by up to 70%. Turgor pressure modeling is done for regular cell geometry, although the cells in the biological petiole have a random orientation. Future work will address the irregular cell orientation for predicting the effect of turgor pressure. Experimental results suggest that the epidermal tissue makes a key contribution to torsional stiffness while its effect on flexural stiffness is minor. From a statistical point of view, the number of experiments should be higher to predict real life petiole structural properties. Accurately predicting the properties of the biological petiole will require further experimentation in order to gain statistically relevant data.

The goal of this work was first to gain insight into the mechanics of petiole structure at multiple length scales, then to apply such lessons to the design of bio-inspired compliant composites based on cellular microstructure. Tissue properties, their relative volume fractions and their orientations appear to govern the overall structural properties of the petiole subjected to both twisting and bending load.

Acknowledgements

The authors would like to thank the staff and administration of the Montreal Botanical Garden. The authors thank Marc-Stéphane Bailleul, Renée Gaudette, Hélène Giguere and Lise Lacouture for helping with the selection of a model species, as well as with collection of samples from that species. The authors also thank Dr. Anja Geitmann, Dr. Denis Barabé and Firas Bou Daher of the Institut de recherche en biologie végétale.

References

- [1] Campbell N A, Reece J B, Mitchell L G. *Biology*, Benjamin Cummings, 2002.
- [2] Niklas K J. *Plant Biomechanics*, The University of Chicago Press, Chicago and London, 1992 .
- [3] Croat Thomas B. L N. The Araceae of Venezuela. *Aroideana*, 1986, **9**, 3–213.
- [4] Wainwright S A, Biggs W D, Currey J D, Gosline J M. *Mechanical Design in Organisms*, Princeton University Press, Princeton, New Jersey, USA, 1982.
- [5] Vogel S. Drag and Reconfiguration of Broad Leaves in High Winds. *Journal of Experimental Botany*, 1989, **40**, 941–948.
- [6] Niklas K J. The mechanical roles of clasping leaf sheaths: Evidence from *Arundinaria tecta* (Poaceae) shoots subjected to bending and twisting forces. *Annals of Botany*, 1998, **81**, 23–34.
- [7] Etnier S A, Vogel S. Reorientation of daffodil (*Narcissus*: Amaryllidaceae) flowers in wind: Drag reduction and torsional flexibility. *American Journal of Botany*, 2000, **87**, 29–32.
- [8] Vogel S. Twist-to-bend ratios of woody structures. *Journal of Experimental Botany*, 1995, **46**, 981–985.
- [9] Koehl M A R. Effects of sea-anemones on flow forces they encounter. *Journal of Experimental Biology*, 1977, **69**, 87–105.
- [10] Pasini D. On the biological shape of the Polygonaceae Rheum Petiole. *International Journal of Design & Nature and Ecodynamics*, 2008, **3**, 1–26.
- [11] Ashby M F. *Materials Selection in Mechanical Design*, Elsevier Butterworth-Heinemann, Burlington, USA, 2005.
- [12] Pasini D. Modelling the micro- and macro-structure efficiencies of a compliant petiole beam. The 4th International Conference on Design and Nature, 2008, **114**, 107–117.
- [13] Pasini D. Bend stiffness of laminate microstructure containing three dissimilar materials. *International Journal of Mechanics and Materials in Design*, 2009, **5**, 175–193.
- [14] Nilsson S B, Hertz C H, Falk S. On the relation between turgor pressure and tissue rigidity. II. theoretical calculations on model systems. *Physiologia Plantarum*, 1958, **11**, 818–837.
- [15] Falk S, Hertz C H, Virgin H I. On the relation between turgor pressure and tissue rigidity. I. experiments on resonance frequency and tissue rigidity. *Physiologia Plantarum*, 1958, **11**, 802–817.
- [16] Lin T T, Pitt R E. Rheology of apple and potato tissue as affected by cell turgor pressure. *Journal of Texture Studies*, 1986, **17**, 291–313.
- [17] Georget D M R, Smith A C, Waldron K W. Modelling of carrot tissue as a fluid-filled foam. *Journal of Materials Science*, 2003, **38**, 1933–1938.
- [18] Glover B J. Plant epidermis. In: Roberts K (ed). *Handbook of Plant Science*, Wiley, Chichester, UK, 2007.
- [19] Jarvis M C. Collenchyma. In: Roberts K (ed). *Handbook of Plant Science*, Wiley, Chichester, UK, 2007.
- [20] Pruyn M L. Parenchyma. In: Roberts K (ed). *Handbook of Plant Science*, Wiley, Chichester, UK, 2007.
- [21] Aizenberg J, Weaver J C, Thanawala M S, Sundar V C, Morse D E, Fratzl P. Skeleton of *Euplectella* sp.: Structural hierarchy from the nanoscale to the macroscale. *Science*, 2005, **309**, 275–278.
- [22] Pasini D. Shape and material selection for optimizing flexural vibrations in multilayered resonators. *Journal of Microelectromechanical Systems*, 2006, **15**, 1745–1758.

- [23] Pasini D. Shape transformers for material and shape selection of lightweight beams. *Materials & Design*, 2007, **28**, 2071–2079.
- [24] Pasini D, Smith D J, Burgess S C. Structural efficiency maps for beams subjected to bending. *Proceeding of the Institution of Mechanical Engeerings, Part L: Journal of Materials: Design and Applications*, 2003, **217**, 207–220.
- [25] Gielis J. A generic geometric transformation that unifies a wide range of natural and abstract shapes. *American Journal of Botany*, 2003, **90**, 333–338.